ABSORPTION LINE SURVEY OF H_3^+ TOWARD THE GALACTIC CENTER SOURCES. II. EIGHT INFRARED SOURCES WITHIN 30 pc OF THE GALACTIC CENTER[1]

MIWA GOTO,[2] TOMONORI USUDA,[3] TETSUYA NAGATA,[4] T. R. GEBALLE,[5] BENJAMIN J. MCCALL,[6] NICK INDRIOLO,[6] HIROSHI SUTO,[7] THOMAS HENNING,[2] CHRISTOPHER P. MORONG,[8] AND TAKESHI OKA[8]

ABSTRACT

Infrared absorption lines of H_3^+, including the metastable $R(3,3)^l$ line, have been observed toward eight bright infrared sources associated with hot and massive stars located in and between the Galactic center cluster and the Quintuplet cluster 30 pc to the east. The absorption lines with high-velocity dispersion arise in the Galaxy's central molecular zone (CMZ) as well as in foreground spiral arms. The temperature and density of the gas in the CMZ, as determined from the relative strengths of the H_3^+ lines, are $T = 200$–300 K and $n \leq 50$–200 cm^{-3}. The detection of high column densities of H_3^+ toward all eight stars implies that this warm and diffuse gaseous environment is widespread in the CMZ. The products of the ionization rate and path length for these sight lines are 1000 and 10 times higher than in dense and diffuse clouds in the Galactic disk, respectively, indicating that the ionization rate, ζ, is not less than 10^{-15} s^{-1} and that L is at least on the order of 50 pc. The warm and diffuse gas is an important component of the CMZ, in addition to the three previously known gaseous environments: (1) cold molecular clouds observed by radio emission of CO and other molecules; (2) hot ($T = 10^4$–10^6 K) and highly ionized diffuse gas ($n_e = 10$–100 cm^{-3}) seen in radio recombination lines, far infrared atomic lines, and radio-wave scattering; and (3) ultrahot ($T = 10^7$–10^8 K) X-ray emitting plasma. Its prevalence significantly changes the understanding of the environment of the CMZ. The sight line toward GC IRS 3 is unique in showing an additional H_3^+ absorption component, which is interpreted as being due to either a cloud associated with circumnuclear disk or the "50 km s^{-1} cloud" known from radio observations. An infrared pumping scheme is examined as a mechanism to populate the (3,3) metastable level in this cloud.

Subject headings: Galaxy: center — ISM: clouds — ISM: lines and bands — ISM: molecules — stars: individual (GC IRS 1W, GC IRS 21, GC IRS 3, GCS 3-2, NHS 21, NHS 22, NHS 25, NHS 42)

1. INTRODUCTION

1.1. *The Central Molecular Zone*

The region of the Galaxy within 200 pc of the center, known as the central molecular zone (CMZ), contains 10% of the Galactic interstellar molecular mass (Morris & Serabyn 1996; Genzel et al. 1994; Mezger et al. 1996, and references therein). The interstellar medium (ISM) in the CMZ is exceptional in many other ways. It is highly turbulent, pervaded by an intense magnetic field (for a review see Morris 2006), contains a multitude of massive stars (e.g., Moneti et al. 1992; Cotera et al. 1999; Muno et al. 2006) and supermassive clusters (e.g., Nagata et al. 1990, 1995; Figer 2004 for a short review), and is also home to numerous highly energetic objects ranging from supernova remnants to cataclysmic variables (CVs; e.g., Muno et al. 2003). The particle densities in its dense molecular clouds are of order 10^4 cm^{-3} and higher. The volume filling factor, f_v, of dense molecular clouds has previously been estimated to be ~10% (Morris & Serabyn 1996), but

is more likely ~1% (Oka et al. 2005) in view of the observed visual extinction of $A_V = 25$–40 mag (Cotera et al. 2000).

If dense molecular clouds only occupy 1% of the CMZ, what interstellar environments make up the remaining 99%? There have been some reports of lower density "diffuse" molecular gas in the intercloud region. Detailed analysis of the $J = 1 \rightarrow 0$ emission lines of CO and C^{18}O by Dahmen et al. (1998) and the $J = 2 \rightarrow 1$ and $J = 1 \rightarrow 0$ emission lines of CO by Oka et al. (1998a) have demonstrated the presence of gas with densities of ~$10^{2.5}$ cm^{-3}. Indeed, Oka et al. (1998a) conclude that CO emission from the Galactic center is dominated by emission from gas of that density. The volume filling factor of $f_v \sim 0.1$ claimed by Morris & Serabyn (1996) may include such gas. In this paper we present evidence for an even lower density molecular environment in which H_2 must still be plentiful but where CO is not abundant. In hindsight, the radio absorption lines with high-velocity dispersion of OH (e.g., Bolton et al. 1964), H_2CO (e.g., Palmer et al. 1969), HCO$^+$ (Linke et al. 1981), and CO (Oka et al. 1998b) may originate in this newly reported environment.

A second candidate to fill the intercloud medium is the ultrahot plasma ($T \sim 10^7$–10^8 K) observed through its diffuse X-ray emission at energies of 0.5–10 keV. The radiation from the plasma is observed in all sight lines to the CMZ (e.g., Koyama et al. 1989, 1996; Yamauchi & Koyama 1993). Lazio & Cordes (1998) suggested that the highly ionized regions with $n_e \sim 10$ cm^{-3} and $T \sim 10^6$ K that are required to explain the λ^2-dependent radio-wave scattering toward the Galactic center are located at the photon-dominated interfaces between the molecular clouds and this ultrahot X-ray-emitting plasma. They proposed that high-density molecular clouds with a volume filling factor of perhaps $f_v \sim 0.1$

are surrounded by the scattering electron gas and the rest of the space is filled with this plasma (see their Fig. 9).

For an environment such as that described above, which is so dominated by ionized gas, "central plasma zone" rather than CMZ would be a more appropriate term for the region. For a variety of reasons the ultrahot and hot plasma cannot occupy the same regions where molecules abound. How those different categories of gas are distributed and how they coexist in the CMZ is not yet understood. Observations of a new astrophysical probe of the CMZ, the infrared absorption spectrum of H$_3^+$ (Geballe & Oka 1996), are beginning to shed fresh light on these questions (Boldyrev & Yusef-Zadeh 2006). Earlier measurements of this molecular ion in the Galactic center by Geballe et al. (1999), Goto et al. (2002), and Oka et al. (2005) were made along only a very few sight lines. In this paper we report and analyze observations of seven transitions of H$_3^+$ along eight sight lines, which provide a more comprehensive diagnostic of the extent and nature of the H$_3^+$-containing gas in the CMZ.

1.2. H$_3^+$ as an Astrophysical Probe

The crucial information obtained from the observations of H$_3^+$ reported here is the product of the ionization rate of molecular hydrogen, ζ, and the aggregate length of the line of sight through the H$_3^+$-containing clouds, L. The simple chemistry of H$_3^+$ allows us to obtain this product from the observed total H$_3^+$ column densities (Oka et al. 2005; Oka 2006b), as described below, under the assumptions that (1) there is a steady state balance between creation and destruction of H$_3^+$ and (2) the dominant supplier of electrons is carbon, all of which is singly ionized.

Creation of H$_3^+$ begins with ionization of H$_2$. Because in interstellar regions where H$_2$ is plentiful the ion-neutral reaction H$_2$ + H$_3^+$ → H$_3^+$ + H is rapid, the limit to the formation of H$_3^+$ is the much slower ionization rate of molecular hydrogen,

$$H_2 + R \rightarrow H_2^+ + e + R'.$$
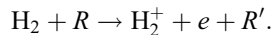
The ionizing rays, R, are dominated by cosmic rays in the Galactic disk (Indriolo et al. 2007, and references therein), but in the CMZ the ionization by X-rays and extreme-ultraviolet (EUV) radiation may be significant. The production rate per unit volume of H$_3^+$ is thus given by $\zeta n(H_2)$, where ζ is the effective ionization rate of H$_2$ including all the aforementioned contributors. In steady state, production of H$_3^+$ balances its destruction, which is dominated by dissociative recombination with electrons,

$$H_3^+ + e \rightarrow 3H \quad \text{or} \quad H_2 + H,$$

and one obtains (Geballe et al. 1999)

$$\zeta n(H_2) = k_e n(H_3^+) n(e),$$

where k_e is the electron recombination rate constant, whose temperature dependent value is $\sim 10^{-7}$ cm^3 s^{-1} (McCall et al. 2004). Replacing the electron density with the atomic carbon density after depletion gives

$$n(e)/n(H_2) = (2/f)[n_C/n_H]_{SV} R_X,$$

where $R_X = 3$–10 is the factor increase in relative carbon abundance at the Galactic center over the solar vicinity, $[n_C/n_H]_{SV}$ (Sodroski et al. 1995), and $f = 2n(H_2)/n_H$ is the fractional density of molecular hydrogen relative to the total number of hydrogen atoms, $n_H = 2n(H_2) + n(H)$. Using $N(H_3^+) = Ln(H_3^+)$ because

of the constancy of $n(H_3^+)$ (e.g., Oka 2006b), we obtain the equation central to the analysis in this paper relating the product ζL to the total H$_3^+$ column density and other measurables,

$$\zeta L = 2k_e[n_C/n_H]_{SV} R_X N(H_3^+)_{total}/f. \tag{1}$$

As discussed by Oka et al. (2005), in the Galactic center the spectrum of H$_3^+$ provides direct information about the temperature and density of the gas. There the relative population of H$_3^+$ in the $(J, K) = (3, 3)$ metastable level, which is 361 K above the lowest $(1,1)$ level (note that $J = 0$ does not exist in the ground vibrational state), is measurable and is a useful thermometer for temperatures of ~ 100–1000 K. Observations of the fractional population in the $(2,2)$ unstable level, from which H$_3^+$ decays to the $(1,1)$ level by spontaneous emission in 27 days (Pan & Oka 1986; Neale et al. 1996), provides a good measure of cloud densities of less than several hundred per cm^3. The lifetime of H$_3^+$ in diffuse clouds is $1/(k_e n_e) \approx 10^9$ s, which is 2 orders of magnitude longer than the collisional timescale with molecular hydrogen. The rotational temperature of H$_3^+$ is therefore maintained via collisions with the ambient H$_2$. The thermalization of H$_3^+$ in interstellar clouds has been modeled by Oka & Epp (2004), who provide H$_3^+$ population ratios $n(3, 3)/n(1, 1)$ and $n(3, 3)/n(2, 2)$ plotted as functions of temperature and density (see their Figs. 2–4).

2. OBSERVATIONS

Bright infrared sources corresponding to dust shells surrounding luminous stars or to hot and bright stars with a dearth of photospheric absorption features were selected from the Sgr A* cluster (Becklin et al. 1978; Krabbe et al. 1995; Tanner et al. 2006), the Quintuplet cluster (Okuda et al. 1990; Nagata et al. 1990), and candidates in their vicinity (Nagata et al. 1993) to use as probes of foreground H$_3^+$ (Table 1). Spectroscopic observations were carried out at the Subaru Telescope over several nights between 2004 July 7 UT and 2004 September 26 UT, using the Infrared Camera and Spectrograph (IRCS; Tokunaga et al. 1998; Kobayashi et al. 2000). The data obtained on 2001 June 16 UT, originally published in Goto et al. (2002), were combined with the newer data. A summary of the observations is given in Table 2.

A curvature-sensing adaptive optics (AO) system (Takami et al. 2004) was used whenever a wave front reference star was available. Use of the AO system significantly increased the throughput of starlight through the narrow (0.15$''$) slit, which was necessary to attain high spectral resolution ($\lambda/\Delta\lambda = 20,000$; $\Delta v = 15$ km s^{-1}). In order to subtract sky and telescope emission, either the telescope itself or the tip-tilt mirror in the AO system was nodded by about 3$''$ along the slit so that the stellar spectrum fell on two different parts of the camera. The slit position was set along the east-west axis in all cases except when nearby faint sources fell onto the slit, which would have hampered a clean sky subtraction.

The angle of cross-dispersing grating in IRCS was adjusted so that as many H$_3^+$ lines as possible were observed in the time available. The major absorption lines essential for the gas diagnostics [the $R(1, 0)$, $R(1, 1)^u$, $R(1, 1)^l$, $Q(1, 0)$, and $Q(1, 1)$ lines from the lowest $(1,1)$ and $(1,0)$ levels, and the $R(3, 3)^l$ and $R(2, 2)^l$ lines from the higher $(3,3)$ and $(2,2)$ levels] were covered in two grating settings. The $Q(1, 0)$ transition at 3.9530 μm was covered by both of the grating settings. Details of the spectral setup are found in Goto et al. (2002).

Standard stars with early spectral types were observed on the same nights through similar airmasses as the Galactic center stars in order to remove the telluric absorption features. Spectroscopic flat fields were obtained from a halogen lamp installed at the Cassegrain port in front of the instrument's entrance window. The

TABLE 1
TARGET LIST

Source	R.A. (J2000.0)	Decl. (J2000.0)	l (deg)	b (deg)	L/L' (mag)	Other Names in SIMBAD	References
GC IRS 21	17 45 40.2	−29 00 31	−0.0561	−0.0468	...	SGR A IRS 21, GC IRS 21	1, 2, 3
GC IRS 3	17 45 39.8	−29 00 24	−0.0552	−0.0448	5.3	BHA 11, GC IRS 3	1, 2, 3
GC IRS 1W	17 45 40.4	−29 00 27	−0.0549	−0.0471	5.5	SGR A IRS 1W, GC IRS 1W	1, 2, 3
NHS 21	17 42 53.8	−28 51 41	+0.0992	−0.0553	4.62	qF 577, [NHS93] 21	4, 5, 6
NHS 22	17 46 05.6	−28 51 41	+0.1199	−0.0482	6.0	[NHS93] 22	4, 5, 6
NHS 42	17 46 08.3	−28 49 55	+0.1481	−0.0426	6.05	qF 578, [NHS93] 42	4, 5, 6
NHS 25	17 46 15.3	−28 50 04	+0.1592	−0.0657	6.2	PISTOL STAR, [NHS93] 25	4, 5, 6
GCS 3-2	17 46:14.7	−28:49:41	+0.1636	−0.0606	2.5	GCS 3-2, [NHS93] 24	4, 5, 6

NOTE.—Units of right ascension are hours, minutes, and seconds, and units of declination are degrees, arcminutes, and arcseconds.
REFERENCES.—(1) Krabbe et al. 1995; (2) Ott et al. 1999; (3) Tanner et al. 2006; (4) Nagata et al. 1990; (5) Nagata et al. 1993; (6) Figer et al. 1999.

sky conditions were fair with the seeing between 0.45″ and 0.75″ at the R band.

3. DATA REDUCTION

The data were reduced using IRAF[9] and custom-written IDL codes. The two-dimensional spectrograms were pair subtracted and then averaged and the pixel responses were normalized by the dark-subtracted flat-field images. Noisy pixels were filtered out based on the pixel statistics, and interpolated prior to spectral extraction. The one-dimensional spectra were obtained using the IRAF aperture extraction package.

The removal of the telluric lines by dividing the data by the spectra of the standard stars was handled by IDL codes that take into account possible observational flaws, including slight shifts

in the wavelengths, differences in airmasses (and therefore depths of telluric absorption lines), slightly different spectral resolutions, fringing of the continua, and saw-toothed features due to the different readout channels. In cases where the flaws were too extreme to be easily corrected, a transmission spectrum calculated by ATRAN (Lord 1992) was used as a substitute to remove the telluric features. The signal-to-noise ratios of the spectra were calculated from the noises on the continua near the H_3^+ absorption lines.

Wavelength calibration was achieved by matching the observed spectra to the model transmission spectrum. The accuracy of the calibration is normally better than 1/10 of one pixel ($\delta v = 0.75$ km s^{-1}) when the signal-to-noise ratio of the observed spectrum is sufficiently high. The radial velocities of the absorption lines observed in the multiple runs were corrected for the orbital motion of the Earth, converted to v_{LSR} using the radial velocity package of IRAF, and added together with appropriate weights according to the signal-to-noise ratios of the spectra. The signal-to-noise ratios after adding up all available data range from 60 to 300.

[9] IRAF is distributed by the National Optical Astronomy Observatories, which are operated by the Association of Universities for Research in Astronomy, Inc., under cooperative agreement with the National Science Foundation.

TABLE 2
SUMMARY OF OBSERVATIONS

SOURCE	EXPOSURE (s)	GRATING[a]		LINE COVERAGE	ATMOSPHERIC STANDARD		UT DATE
		ECH	XDP		Name	Spectral Type	
GC IRS 21	1800	11050	2800	$R(2,2)^l$, $R(1,1)^u$, $R(1,0)$, $Q(1,1)$, $Q(1,0)$	HR 7528	B9.5 IV	2004 Jul 28
	2400	5050	3500	$R(3,3)^l$, $R(1,1)^l$, $Q(1,0)$	HR 6378	A2 V	2004 Sep 2
GC IRS 3	360	8350	6100	$R(1,1)^u$, $R(1,0)$, $R(1,1)^l$, $Q(1,1)$, $Q(1,0)$	HR 7924 (α Cyg)	A2 Iae	2001 Jun 16
	1440	4400	5200	$R(3,3)^l$, $R(1,1)^l$	HR 7924 (α Cyg)	A2 Iae	2001 Jun 16
	3120	11050	2800	$R(2,2)^l$, $R(1,1)^u$, $R(1,0)$, $Q(1,1)$, $Q(1,0)$	HR 7001 (α Lyr)	A0 V	2004 Jul 7
	2400	5050	3500	$R(3,3)^l$, $R(1,1)^l$, $Q(1,0)$	HR 7001 (α Lyr)	A0 V	2004 Jul 8
	3000	11050	2800	$R(2,2)^l$, $R(1,1)^u$, $R(1,0)$, $Q(1,1)$, $Q(1,0)$	HR 7121	B2.5 V	2004 Sep 25
	1280	11050	2800	$R(2,2)^l$, $R(1,1)^u$, $R(1,0)$, $Q(1,1)$, $Q(1,0)$	HR 7121	B2.5 V	2004 Sep 26
GC IRS 1W	2560	5050	3500	$R(3,3)^l$, $R(1,1)^l$, $Q(1,0)$	HR 7001 (α Lyr)	A0 V	2004 Jul 27
	2560	11050	2800	$R(2,2)^l$, $R(1,1)^u$, $R(1,0)$, $Q(1,1)$, $Q(1,0)$	HR 7528	B9.5 IV	2004 Jul 27
NHS 21	3600	11050	2800	$R(2,2)^l$, $R(1,1)^u$, $R(1,0)$, $Q(1,1)$, $Q(1,0)$	HR 7001 (α Lyg)	A0 V	2004 Jul 8
	3600	5050	3500	$R(3,3)^l$, $R(1,1)^l$, $Q(1,0)$	HR 6378	A2 V	2004 Jul 8
NHS 22	1200	11050	2800	$R(2,2)^l$, $R(1,1)^u$, $R(1,0)$, $Q(1,1)$, $Q(1,0)$	HR 7121, ATRAN	B2.5 V	2004 Sep 4
	1200	5050	3500	$R(3,3)^l$, $R(1,1)^l$, $Q(1,0)$	HR 7121, ATRAN	B2.5 V	2004 Sep 4
NHS 42	1920	11050	2800	$R(2,2)^l$, $R(1,1)^u$, $R(1,0)$, $Q(1,1)$, $Q(1,0)$	HR 7924 (α Cyg)	A2 Iae	2004 Jul 27
	1920	5050	3500	$R(3,3)^l$, $R(1,1)^l$, $Q(1,0)$			2004 Jul 27
NHS 25	1200	5050	3500	$R(3,3)^l$, $R(1,1)^l$, $Q(1,0)$	HR 7121	B2.5 V	2004 Sep 4
	1200	11050	2800	$R(2,2)^l$, $R(1,1)^u$, $R(1,0)$, $Q(1,1)$, $Q(1,0)$	HR 7121	B2.5 V	2004 Sep 4
GCS 3-2	120	8350	6100	$R(1,1)^u$, $R(1,0)$, $R(1,1)^l$, $Q(1,1)$, $Q(1,0)$	HR 7528	B9.5 IV	2001 Jun 16
	240	4400	5200	$R(3,3)^l$, $R(1,1)^l$, $Q(1,0)$	HR 7528	B9.5 IV	2001 Jun 16
	1344	11050	2800	$R(2,2)^l$, $R(1,1)^u$, $R(1,0)$, $Q(1,1)$, $Q(1,0)$	HR 7001 (α Lyr)	A0 V	2004 Jul 7
	1344	5050	3500	$R(3,3)^l$, $R(1,1)^l$, $Q(1,0)$	HR 7001 (α Lyr)	A0 V	2004 Jul 7

[a] ECH and XDP denote the angles of echelle and cross-dispersing gratings in the instrumental coding unit.
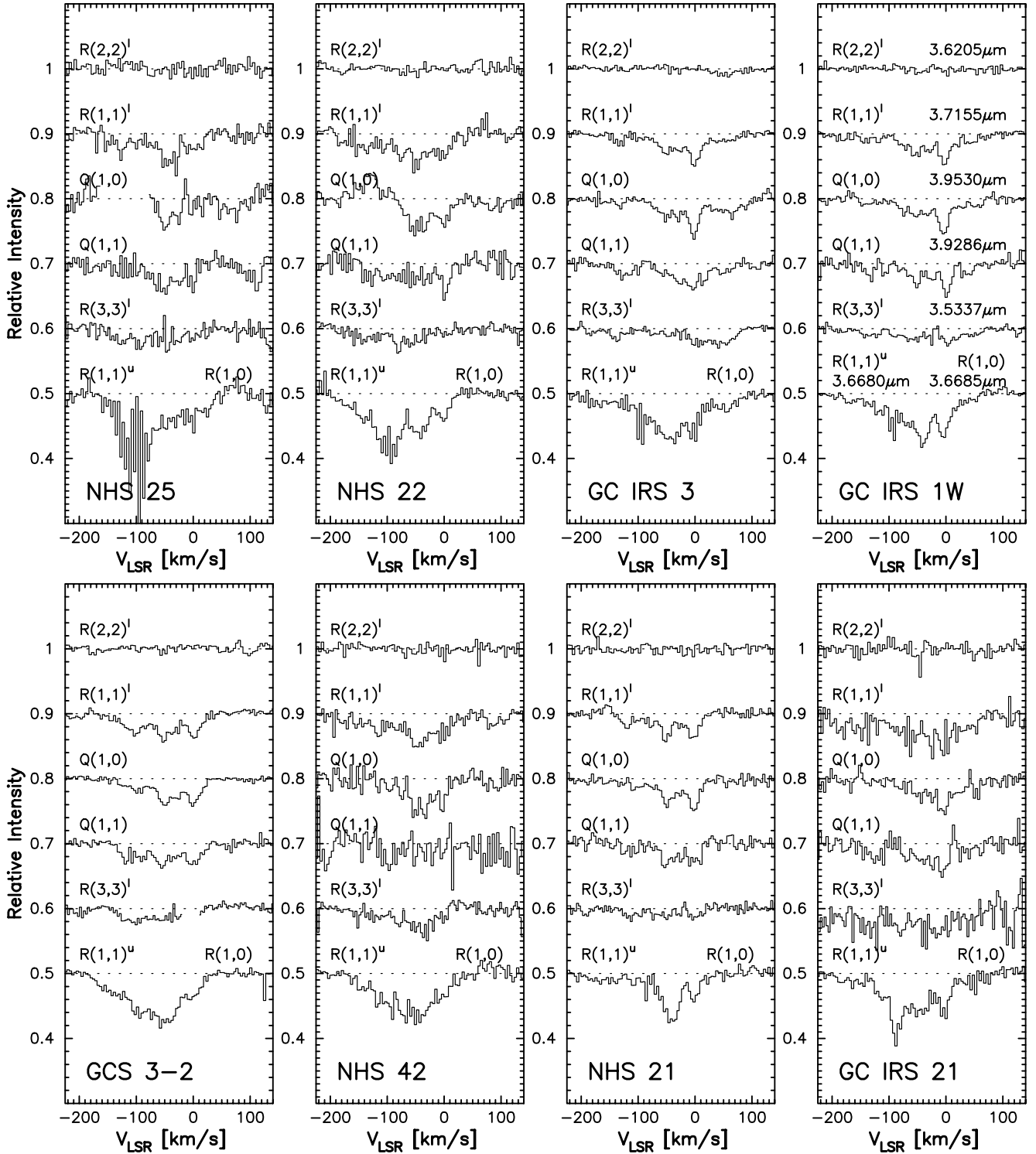
Fig. 1.—Spectra of H_3^+ toward eight sources in the Central Molecular Zone. The $R(1, 1)^u$ and $R(1, 0)$ absorptions in the bottom lines are separated by 35 km s^{-1} and the profiles overlap. The telluric absorption of N_2O interferes heavily with the wavelength interval near $Q(1, 1)$, causing the low signal-to-noise ratios. The gap in the spectrum of NHS 25 in the $Q(1, 0)$ line corresponds to a strong atomic emission line, probably that of Si II.

The seven most relevant lines for this study are shown in Figure 1. For the Pistol Star, NHS 25, and possibly more weakly for NHS 22, the $Q(1, 0)$ line at 3.9530 μm is overlapped at low wavelength with an atomic emission line. This wavelength region is omitted for NHS 25 in Figure 1. The atomic emission matches the Si II lines at 3.9477–3.9499 μm compiled in the NIST table.[10]

4. RESULTS

4.1. *Overview*

All five of the absorption lines [$R(1, 0)$, $R(1, 1)^u$, $R(1, 1)^l$, $Q(1, 0)$, and $Q(1, 1)$] that originate from the lowest para- and orthorotational levels, $(J, K) = (1, 1)$ and $(1, 0)$, were detected in all sight lines. In each sight line the line profiles of these transitions are basically the same (Fig. 1), showing a broad trough of absorption primarily at negative radial velocities, and several sharp absorption minima, which we attribute to intervening clouds in the foreground spiral arms, as did Oka et al. (2005) for GCS 3-2.

The 3.5337 μm $R(3, 3)^l$ line from the (3,3) metastable level was detected in all targets. In nearly every case it occurs largely at negative radial velocities. Its profile is broad and rather smooth, with a width approaching 150 km s^{-1}, and with no sharp features. H_3^+ lines of such width have never been seen in the Galactic disk. Moreover, searches for the $R(3, 3)^l$ line in the disk along sight lines where the H_3^+ lines from the lowest two levels have clearly been observed (Geballe & Oka 1996; McCall et al. 1998, 2002; Geballe et al. 1999; Indriolo et al. 2007) have been unsuccessful (Oka et al. 2005). For these reasons and following Oka et al. (2005), we attribute the entire $R(3, 3)^l$ absorption to the gas in the CMZ. The $R(3, 3)^l$ line profile mimics the broad trough in the $J = 1$ H_3^+ absorption line profiles. We use this resemblance to differentiate between the absorptions in the CMZ and those in the spiral arms.

The $R(2, 2)^l$ line at 3.6205 μm was detected in one sight line only, that toward GC IRS 3, and only at velocities near +50 km s^{-1}. Because this is the first time that this line has been detected and because absorption by it is only 1%–2%, we have carefully examined its reality. Two telluric CH_4 lines line at 2762.48 cm^{-1} (3.61994 μm) and 2761.36 cm^{-1} (3.62141 μm) with peak absorption strengths of 20%–30% overlap the $R(2, 2)^l$ line; incomplete cancellation of them could cause absorption features near the observed feature. However, the wavelength match is not precise, and moreover, the width of the $R(2, 2)^l$ line (40–60 km s^{-1}) is twice that of each of the telluric lines, which are nearly unresolved. As a further check we obtained independent observations of GC IRS 3 from the United Kingdom Infrared Telescope (UKIRT) in 2004 September and 2005 July, using the echelle in the facility spectrograph CGS4. Although somewhat different in detail, the UKIRT observations consistently show a 1%–2% absorption dip at the same wavelength as the Subaru data. Thus the detection of this line toward GC IRS 3 is genuine. All observed spectra of the $R(2, 2)^l$ line in GC IRS 3 are shown in Figure 2, together with the $R(3, 3)^l$ and $R(1, 1)^l$ absorption lines.

In contrast to the Galactic disk where the detectable presence of H_3^+ is limited to relatively few sight lines and their narrow angular proximity, every sight line observed toward the CMZ has abundant H_3^+. Although the targets presented here are within 30 pc of Sgr A* in projected distance, the lengths of all of the absorbing columns of H_3^+ are very large (significantly larger than this separation), as discussed below (see also Oka et al. 2005), and the observed velocity dispersion is very large, with absorption occurring from −150 km s^{-1} to +20 km s^{-1}. This range approximately
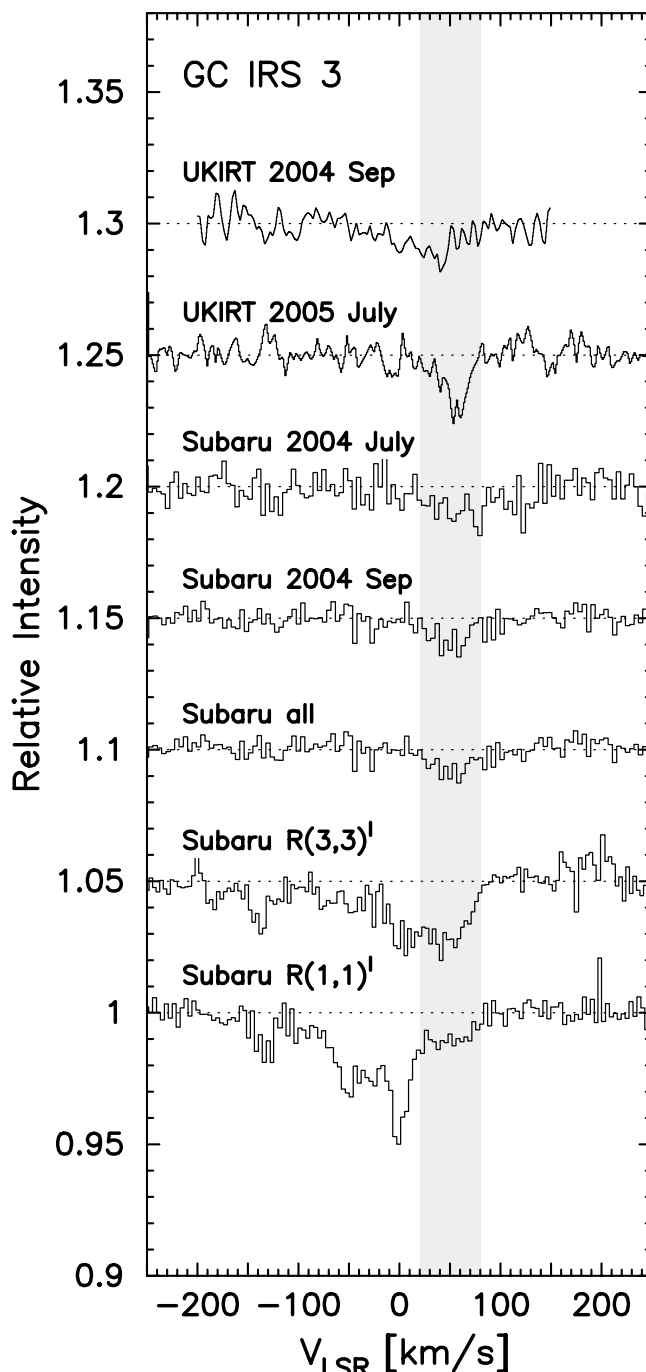
FIG. 2.—Spectra of the $R(2, 2)^l$ line at 3.6205 μm toward GC IRS 3 that was obtained at Subaru and UKIRT. The $R(3, 3)^l$ and $R(1, 1)^l$ lines observed at Subaru are also shown.

matches the entire span of the radial velocity of the gas in the CMZ on the front side of the center (Sawada et al. 2004). These characteristics suggest that the gas containing the observed H_3^+ is not located in well-separated entities, but is continuous with a large volume filling factor. The large column densities of H_3^+ in all sight lines are most obvious in the bottom lines of Figure 1, where two of the strong H_3^+ spectral lines from the (1,1) and (1,0) levels overlap and yield a blended feature of large equivalent width.

4.2. H_3^+ *Equivalent Widths and Column Densities*

H_3^+ lines from the $J = 1$ levels are composites of absorption in the CMZ and in foreground spiral arms. Oka et al. (2005) separated
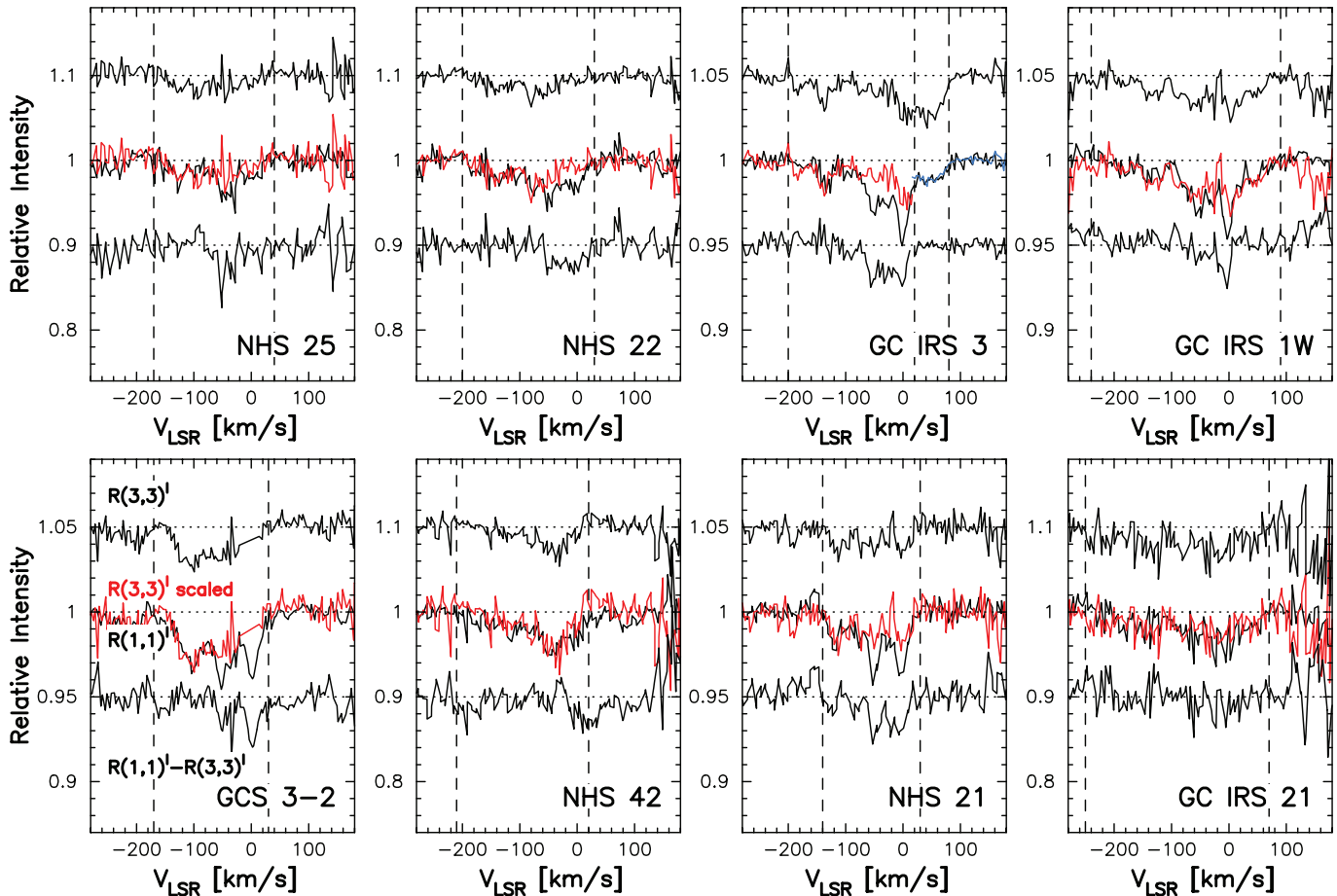
Fig. 3.— Scaling the $R(3,3)^l$ absorption (*top line in each panel*) to match the absorption trough of the $R(1,1)^l$ absorption (*middle line in black*). The scaled $R(3,3)^l$ line is overlaid in red with $R(1,1)^l$, and the difference spectrum is shown in the bottom line. Vertical lines indicate the range of velocities where the profiles were scaled. For GC IRS 3, the scaling is done separately in the two velocity ranges, −200 to 20 km s^{-1} (*red lines*) and 20 to 80 km s^{-1} (*blue line*).

the two components of the $R(1,1)^l$ absorption profile in GCS 3-2 by using the 2.3 μm $v = 2-0$ $R(1)$ line of CO, which is composed of sharp absorption features at the radial velocities (−50, −30, and 0 km s^{-1}) of foreground spiral arms with little or no CMZ component. The sharp features in the H$_3^+$ absorption profile, which mimic the CO spectrum, were subtracted from the $R(1,1)^l$ line and the remainder was ascribed to H$_3^+$ in the CMZ (see Fig. 4 of Oka et al. 2005).

We found that this method was not effectively applicable for the spectra in Figure 1 because of the lower resolution of the IRCS (by a factor of 3) compared to the Phoenix Spectrometer of the Gemini South Observatory, and the low signal-to-noise ratios of spectra toward targets that were fainter than GCS 3-2. We used an alternative method for separation, in which we assume for each star that the velocity profile of the trough in the $J = 1$ lines is a scaled version of the $R(3,3)^l$ profile. The method is depicted in Figure 3. It crudely assumes uniform physical conditions in the absorbing clouds along the line of sight. We used it to separate the CMZ and spiral arm components of the $Q(1,0)$ line as well as the $R(1,1)^l$ line. We ignore the detailed velocity profiles of the observed spectra, and list integrated absorptions of the $R(1,1)^l$ line and their ratios in the CMZ to the total (CMZ plus spiral arms). This ratio is also the ratio of column densities. We tested the method for GCS 3-2, for which Oka et al. (2005) used the high-resolution spectrum obtained by Phoenix at the Gemini South Observatory and reported the ratio $[N(1,1)_{GC}/N(1,1)_{total} = 0.68]$ by a different method of analysis using CO spectrum; the agreement

is satisfactory. The interference with the $Q(1,0)$ line by the atomic emission for NHS 25 mentioned in § 3 does not seriously hamper the measurement since the scaling of the $R(3,3)^l$ line to the $Q(1,0)$ line is not much affected. The ratio of the equivalent width of the CMZ component to the total ranges from 0.5 to 0.9 for the eight sight lines.

The sight line toward GC IRS 3 is exceptional in that it passes through two different categories of gas. In addition to the gas with mostly negative velocity common to all eight targets, it shows absorption at +50 km s^{-1}. This absorption is unique in two other ways: (1) it is the only gas in which the $R(2,2)^l$ line is observable (indicating that the gas producing this velocity feature is higher in density than the gas seen at other velocities); and (2) it is the only gas for which the column density of the (3,3) metastable level is definitely higher than in the (1,1) ground level. Therefore we consider the +50 km s^{-1} absorption separately. Measured equivalent widths of all spectral lines are listed in Table 3. For those transitions starting from the (1,1) level, both total equivalent widths and equivalent widths for the part of the absorption originating in the CMZ are provided.

The H$_3^+$ column densities in the (1,0), (1,1), (3,3), and (2,2) levels were calculated from the equivalent widths of the $Q(1,0)$, $R(1,1)^l$, $R(3,3)^l$, and $R(2,2)^l$ lines, respectively, as in Geballe et al. (1999), from the equation $W_\lambda = (8\pi^3/3h\nu)N_{level}|\mu|^2$, using the theoretical line strengths $|\mu|^2$ provided by J. K. G. Watson (also calculable from the list of Neale et al. 1996). The results are given in Table 4. The column density corresponding to the

TABLE 3
EQUIVALENT WIDTHS OF ABSORPTION LINES

Source	Velocity Range[a] v_1 (km s^{-1})	Velocity Range[a] v_2 (km s^{-1})	W_λ total[b] $R(1,1)^l$ (10^{-5} μm)	Scaling Factor[c] $R(3,3)^l \rightarrow R(1,1)^l$	Scaling Factor[c] $R(3,3)^l \rightarrow Q(1,0)$	W_λ in Galactic Center[d] $R(1,1)^l$ (10^{-5} μm)	W_λ in Galactic Center[d] $Q(1,0)$ (10^{-5} μm)	W_λ in Galactic Center[d] $R(3,3)^l$ (10^{-5} μm)	W_λ in Galactic Center[d] $R(2,2)^l$ (10^{-5} μm)	$N(1,1)_{GC}/N(1,1)_{total}$[e]
GC IRS 21	−250	70	6.7 ± 2.7	0.90	0.55	6.1 ± 2.4	3.7 ± 1.0	6.8 ± 3.4	<2.2	0.91 ± 0.40
GC IRS 3	−200	20	4.0 ± 0.5	1.00	0.60	2.4 ± 0.5	1.4 ± 0.3	2.4 ± 0.5	<0.4	0.59 ± 0.12
GC IRS 1W	−240	90	4.5 ± 0.8	1.20	1.00	3.9 ± 1.0	3.3 ± 1.0	3.3 ± 0.8	<0.9	0.88 ± 0.18
NHS 21	−140	30	3.6 ± 0.5	1.25	1.00	2.0 ± 0.6	1.6 ± 0.6	1.6 ± 0.4	<0.6	0.54 ± 0.13
NHS 22	−200	30	5.9 ± 1.2	1.35	1.20	3.7 ± 1.7	3.3 ± 1.8	2.7 ± 0.7	<1.0	0.63 ± 0.21
NHS 42	−210	20	6.4 ± 1.1	1.60	1.45	3.9 ± 1.8	3.5 ± 2.5	2.4 ± 1.1	<1.1	0.61 ± 0.17
NHS 25	−170	40	4.2 ± 1.3	1.20	0.80	2.5 ± 1.5	1.7 ± 1.3	2.1 ± 1.5	<1.0	0.60 ± 0.31
GCS 3-2	−170	30	5.5 ± 0.4	1.35	0.70	3.7 ± 0.5	1.9 ± 0.2	2.7 ± 0.5	<0.8	0.68 ± 0.07
GC IRS 3 (50 km s^{-1})[f]	20	80	0.7 ± 0.1	0.50	0.65	0.7 ± 0.1	0.9 ± 0.1	1.4 ± 0.1	0.5 ± 0.2	0.93 ± 0.15

[a] Equivalent widths are measured by integrating absorption intensity in the range between v_1 and v_2.
[b] The total equivalent width of the $R(1, 1)^l$ line.
[c] Scaling factor to match the $R(3, 3)^l$ absorption lines to the troughs of the $R(1, 1)^l$ lines (see Fig. 3).
[d] Equivalent widths of H$_3^+$ absorption troughs due to H$_3^+$ in the CMZ.
[e] Ratio of equivalent width in the CMZ to the total equivalent width.
[f] Equivalent width of GC IRS 3 in the 20–80 km s^{-1} range where the $R(2, 2)^l$ absorption is detected.

TABLE 4

COLUMN DENSITIES OF H_3^+ IN THE GALACTIC CENTER

| Source | $N(H_3^+)_{level}$[a] | | | | Relative Population[a] | | $n(H_2)$ | $T(H_2)$ | $N(H_3^+)_{total}$ | $(\zeta L)_{min}$ | L[b] |
	$N(1,1)$ (10^{14}cm^{-2})	$N(1,0)$ (10^{14}cm^{-2})	$N(3,3)$ (10^{14}cm^{-2})	$N(2,2)$ (10^{14}cm^{-2})	$N(3,3)/N(1,1)$	$N(3,3)/N(2,2)$	(cm^{-3})	(K)	(10^{14}cm^{-2})	(10^3cm s^{-1})	(pc)
GC IRS 21	28.1 ± 12.3	9.0 ± 4.4	24.2 ± 12.1	<8.3	0.86 ± 0.57	>2.93	<125	150−450	61.3 ± 17.8	451 ± 131	146 ± 43
GC IRS 3	10.8 ± 2.1	3.4 ± 1.3	8.4 ± 1.9	<1.6	0.78 ± 0.23	>5.36	<50	225−400	22.5 ± 3.2	166 ± 23	54 ± 8
GC IRS 1W	18.1 ± 3.8	7.9 ± 2.4	11.7 ± 3.0	<3.3	0.65 ± 0.21	>3.53	<75	200−300	37.6 ± 5.4	277 ± 40	90 ± 13
NHS 21	8.9 ± 2.2	3.7 ± 1.5	5.6 ± 1.4	<2.3	0.62 ± 0.22	>2.44	<125	175−275	18.2 ± 3.1	134 ± 22	44 ± 7
NHS 22	16.9 ± 5.6	7.9 ± 3.5	9.7 ± 2.7	<3.6	0.57 ± 0.25	>2.73	<100	150−275	34.5 ± 7.2	254 ± 53	82 ± 17
NHS 42	17.7 ± 5.1	8.4 ± 4.1	8.6 ± 4.1	<4.0	0.49 ± 0.27	>2.13	<100	125−250	34.6 ± 7.7	255 ± 57	83 ± 18
NHS 25	11.4 ± 5.9	4.0 ± 3.8	7.4 ± 5.3	<3.9	0.65 ± 0.57	>1.89	<175	100−300	22.8 ± 8.8	168 ± 64	54 ± 21
GCS 3−2	17.0 ± 1.7	4.6 ± 0.8	9.8 ± 1.6	<3.0	0.57 ± 0.11	>3.21	<80	200−250	31.4 ± 2.5	231 ± 18	75 ± 6
GC IRS 3 (50 km s^{-1})	3.2 ± 0.5	2.1 ± 0.4	4.9 ± 0.5	1.9 ± 0.6	1.55 ± 0.29	2.61 ± 0.50	150−350	350−500	10.2 ± 0.8	75 ± 6	24 ± 2

[a] All column densities are for the CMZ only.
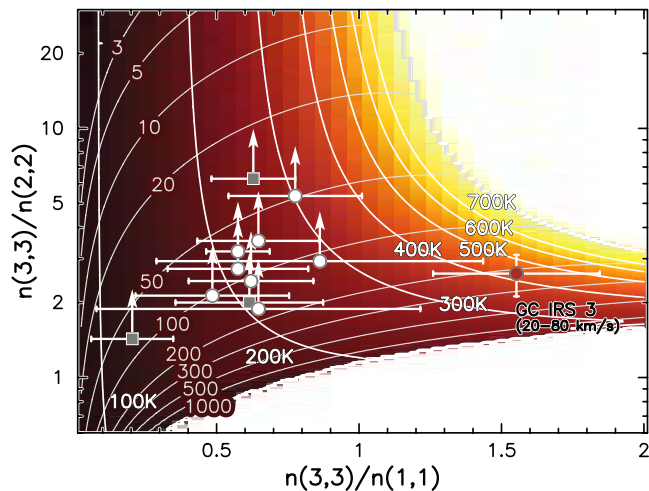[b] Using $\zeta = 1 \times 10^{-15}$ s^{-1}.

FIG. 4.—Temperature and density plotted in filled circles as functions of population ratios $n(3,3)/n(1,1)$ and $n(3,3)/n(2,2)$, obtained by inverting the diagram of Oka & Epp (2004). Temperature is indicated by thick white lines and density by thin lines. The estimated uncertainties in $n(3,3)/n(1,1)$ are shown by error bars. Velocity-resolved data of GCS 3-2 from Oka et al. (2005) are shown as filled squares for comparison.

50 km s^{-1} absorption toward GC IRS 3 is listed separately at the bottom of the table. The total column densities $N(H_3^+)_{total}$ are simply the sum of column densities of the (1,1), (1,0), (3,3), and (2,2) levels, since modeling of the thermalization (Oka & Epp 2004) shows that they are the only levels significantly populated at the temperatures and densities of the region.

For broad spectral lines such as those treated in this paper, uncertainties in the equivalent widths result mainly from the uncertainties in defining the continuum level rather than the standard deviations of individual data points. The listed uncertainties were estimated by multiplying the standard deviation of the continuum level by the width of the relevant velocity range.

4.3. Temperature and Density

The column densities given in Table 4 were used to determine the temperatures, T, and densities, n, of the gas based on the steady state calculation by Oka & Epp (2004). Their diagram, in which the values of the population ratios $n(3,3)/n(1,1)$ and $n(3,3)/n(2,2)$ are plotted as functions of T and n (their Fig. 4), is inverted in our Figure 4 so that the observed population ratios can be used directly to determine T and n. The population ratios toward GCS 3-2 from the velocity resolved data by Oka et al. (2005) are included in the figure for comparison. Most of the clouds in the Galactic center fall in the narrow parameter region of the T-n diagram, 200 K < T < 300 K and $n \leq$ 50–200 cm^{-3}, with the sole exception being the +50 km s^{-1} component toward GC IRS 3, for which a higher temperature of $\sim$ 400 K and a density of 200 cm^{-3} were found.

The upper limits to the number densities in Table 4 are based on the upper limits to the $R(2,2)^l$ line equivalent widths. Lower limits may be roughly estimated from the total extinction of $A_V \sim$ 30 mag reported by Cotera et al. (2000) toward the Quintuplet and Central clusters and the estimate by Whittet et al. (1997) that the visual extinction of the diffuse ISM toward the Galactic center is $\sim$20 mag, that is, $E(B-V) \sim 6.5$. Ascribing all of the latter to the CMZ and using the standard conversion factor from $E(B-V)$ to $N(H)$ (Bohlin et al. 1978) gives $N(H_2) \sim 2 \times 10^{22}$ cm^{-2}. Assuming $L = 100$ pc yields $n(H_2) \sim 60$ cm^{-3}. This shows that the gas density is not much lower than the upper limit. Indeed, the very existence of observable H_3^+ also argues against much lower den-

sities, in which conditions it would be difficult for the H_2, which is needed to produce H_3^+, to exist.

5. DISCUSSION

5.1. The Ionization Rate

An estimate of the ionization rate, ζ, in the Galactic center is the most important result of these H_3^+ observations. To avoid confusion, we use $\zeta(H)$ and $\zeta(H_2)$ for the ionization rates of H and H_2, respectively, in the Galactic disk where ionization is mainly due to cosmic rays. We use ζ for the rate in the CMZ where the effect of X-rays and far-ultraviolet (FUV) radiation may be significant. $\zeta(H)$ and $\zeta(H_2)$ are related approximately as $\zeta(H_2) = 2\zeta(H)$ (Dalgarno 2006).

Early studies of the cosmic-ray ionization rate were made in order to understand the physical state of the ISM and its heating mechanisms (Hayakawa et al. 1961; Spitzer & Tomasko 1968; Field et al. 1969). Spitzer & Tomasko (1968) reported a minimum value of $\zeta_f = 6.8 \times 10^{-18}$ s^{-1} from an extrapolation of the cosmic-ray spectrum observed at Earth, and an upper limit of 1.2×10^{-15} s^{-1} calculated from an assumed supernova frequency. Their ζ_f is the total ionization rate for atomic hydrogen including the effect of secondary electrons, written here as $\zeta(H)$. The most recent measurement of $\zeta(H)$, reported by Webber (1998) using data from the *Voyager* and *Pioneer* spacecraft at distances up to 60 AU from the Sun, is $\zeta(H) \geq (3-4) \times 10^{-17}$ s^{-1}, which should replace the lower limit used by Spitzer & Tomasko (1968).

With the advent of the *Copernicus* satellite and its FUV spectrometer, which allowed FUV studies of chemical abundances in the diffuse ISM (for a review; Spitzer & Jenkins 1975), column densities of molecules and radicals such as HD and OH could be measured. The reaction sequences leading to the creation of these two molecules start from H^+ and are thus useful for estimating $\zeta(H)$. Values of $\zeta(H)$ determined in this way (O'Donnell & Watson 1974; Black & Dalgarno 1977; Hartquist et al. 1978) are mostly a few times 10^{-17} s^{-1}, comparable to the lower limit given above. The comprehensive model of the diffuse ISM by van Dishoeck & Black (1986) suggested a somewhat higher value of $\zeta(H) \approx 7 \times 10^{-17}$ s^{-1}. However, they used an H_3^+ dissociative recombination rate constant 1000 times lower than the current value, which was popular in some circles at the time. They noted that if the 1000 times higher constant were to be used, the value of $\zeta(H)$ would need to be increased by a factor of $\sim$10.

The formation and destruction mechanisms for H_3^+ are the simplest of all astrophysical probes of the ionization rate, and this makes H_3^+, when detectable, a powerful tool for measuring the ionization rate. While the H_3^+ column densities observed in dense clouds, $(0.4-2.3) \times 10^{14}$ cm^{-2}, are consistent with $\zeta(H_2)$ on the order of 3×10^{-17} s^{-1} (Geballe & Oka 1996; McCall et al. 1999), the surprisingly high $N(H_3^+)$ observed in diffuse clouds, comparable to those in dense clouds in spite of their 10 times smaller visual extinction (McCall et al. 1998, 2002; Geballe et al. 1999), require an order of magnitude higher $\zeta(H_2)$. Crucial to this conclusion are the laboratory measurements of the dissociative recombination rate constant k_e in equation (1) (Amano 1988; Larsson et al. 1993; Larsson 2000; McCall et al. 2003, 2004).

Together, McCall et al. (2002) and Indriolo et al. (2007) have carried out a survey of H_3^+ in the diffuse ISM toward 29 nearby stars. H_3^+ was detected in 14 of these sight lines with column densities of $(0.6-6.5) \times 10^{14}$ cm^{-2}. For these diffuse clouds the product ζL is in the range $(0.5-4.4) \times 10^4$ cm s^{-1}. Separating ζ and L is not straightforward. Based on various methods of estimating L, which gave values of 2.2–31 pc for different clouds, the cosmic-ray ionization rates were found to be in the range

$\zeta(H_2) = (1.2\text{–}7.4) \times 10^{-16}$ s^{-1}, with an average of 5×10^{-16} s^{-1}. Note that the primary ionization rate of H, ζ_p, used by Indriolo et al. (2007) is related to $\zeta(H_2)$ by $2.3\zeta_p = \zeta(H_2)$ (Glassgold & Langer 1974). This has established that the cosmic-ray ionization rate in diffuse clouds is an order of magnitude higher than in dense clouds. This result might be understandable in view of attenuation of soft components of cosmic rays in dense clouds (Cravens & Dalgarno 1978), if a large flux of low energy cosmic rays is ubiquitous in the Galaxy (McCall et al. 2003), or if higher energy cosmic rays are trapped by Alfvén waves in diffuse clouds (Padoan & Scalo 2005). The discrepancy between the high $\zeta(H_2)$ and previous low $\zeta(H)$ values determined from HD and OH has been explained by Liszt (2003) as being due to neutralization of H$^+$ by charge exchange with small grains that were considered in the previous studies, in which the neutralization of H$^+$ was assumed to be due to much slower radiative recombination with electrons.

As seen in Table 3, the total column density of H$_3^+$ in the CMZ toward the eight observed stars ranges over $(1.8\text{–}6.1) \times 10^{15}$ cm^{-2}, more than an order of magnitude higher than the column densities in diffuse clouds in the Galactic disk, suggesting even higher values of ζ and L. Since we are interested in setting the minimum value of both ζ and L, we use the maximum value of $f = 1$ and the minimum value of $R_X = 3$ (Sodroski et al. 1995; Arimoto et al. 1996) in equation (1) and obtain the numerical expression

$$(\zeta L)_{\min} = 7.4 \times 10^{-11} \text{ cm}^3 \text{ s}^{-1} \ N\left(H_3^+\right)_{\text{total}}. \tag{2}$$

To obtain equation (2), we have used $k_e = 7.7 \times 10^{-8}$ cm^3 s^{-1} calculated for $T = 250$ K from the temperature dependence reported by McCall et al. (2004), assuming the same electron temperature as the gas temperature, which may be justified in view of the fast thermalization of electrons with molecules and atoms. We used the C to H ratio in the solar vicinity of 1.6×10^{-4} given by Sofia et al. (2004), which is close to the value of 1.4×10^{-4} determined directly from infrared spectra of CO and H$_2$ toward an embedded young star, NGC 2024 IRS 2 (Lacy et al. 1994), and 1.3×10^{-4}, found by Usuda et al. (2008, private communication) with the same technique but toward NGC 7538 IRS 1 in the outer Galaxy. The observed $N(H_3^+)_{\text{total}}$ yield lower limits for ζL, $(\zeta L)_{\min} = (1.3\text{–}4.5) \times 10^5$ cm s^{-1}. Although lower limits, the values of $(\zeta L)_{\min}$ are 1000 times higher than values of ζL determined for dense clouds (McCall et al. 1999) and 10 times higher than values for diffuse clouds in the Galactic disk (Indriolo et al. 2007). We cannot cleanly separate ζ and L based on current understanding of the CMZ, but discuss two extreme cases in the following sections.

5.2. The Case of Large L in the CMZ

Oka et al. (2005) favored a large L and hence a high volume filling factor for the newly found warm and diffuse molecular gas. This was not only because the $R(3, 3)^l$ metastable lines with large velocity widths and similar velocity profiles were detected along all eight lines of sight toward sources scattered over 30 pc in projected distance from Sgr A*, but also because the deduced T and n of the gas were similar in all cases. The latter suggests that the absorbing diffuse material is continuous rather than contained in several separate entities. Further support for this interpretation is that the range of H$_3^+$ absorption velocities in each sight line spans the entire range of velocities observed at radio and millimeter wavelengths with large apertures and interpreted as coming from the front side of the CMZ. Extending spectroscopy of H$_3^+$ over more widely spaced sight lines in the CMZ will constitute a more definitive test of the filling factor. A long path length may also be

favored over high ionization, in that there are limits to the value of ζ for efficient production of H$_3^+$, as discussed in the next subsection.

L is unlikely to be significantly larger than the radius of the CMZ, which for the region of interest is $\sim$130 pc, as estimated using Figure 11b of Sawada et al. (2004). Setting $L = 100$ pc, close to this maximum permissible value, the aforementioned range of values of $(\zeta L)_{\min}$ yields the lower limits $\zeta_{\min} = (0.4\text{–}1.5) \times 10^{-15}$ s^{-1} for the various sight lines. For lower values of f and higher values of R_X, $\zeta_{\min}$ will be higher.

The large extent of the warm and diffuse molecular gas postulated above conflicts with the previous concept of the gas in the CMZ represented, for example, in Figure 9 of Lazio & Cordes (1998), where the ultrahot X-ray emitting plasma fills the CMZ. The warm and diffuse gas revealed in this paper cannot coexist with the ultrahot plasma because the plasma electrons will be immediately cooled and molecules will be destroyed. Thus in the above model the volume filling factor of the ultrahot gas would be reduced by a large factor.

The large extent of the ultrahot plasma gas in the CMZ was proposed because of observations of extensive X-ray emission near the Galactic center (e.g., Koyama et al. 1989, 1996; Yamauchi & Koyama 1993). Sunyaev et al. (1993) and Markevitch et al. (1993) observed similar X-ray emission, but interpreted it differently in view of the difficulty of confining such a hot gas with the gravitational potential of the Galactic center, and of the extraordinarily large energy input required to maintain the high temperature. With the advent of the *Chandra* X-ray satellite, a great many X-ray point sources have been resolved in the Galactic center. These have been interpreted as explaining all (Wang et al. 2002), or a significant fraction (Muno et al. 2003), of the observed intense X-rays as being due to stellar sources such as CVs and young stellar objects. Additional observational reports also argue against the ultrahot plasma, based on the close correlation between the stellar distribution and the observed intensities of the X-rays in the Galactic center (e.g., Warwick et al. 2006) and in the Galactic ridge (e.g., Revnivtsev et al. 2006). However, interpretation of the X-ray emission remains controversial (e.g., Muno et al. 2004; Morris & Nayakshin 2006; Koyama et al. 2007).

Yet another category of high-temperature gas observed in the CMZ is the hot gas observed in recombination lines and other phenomena. Lazio & Cordes (1998) studied the λ^2-dependent hyperstrong radio-wave scattering and free-free radio emissions and absorptions and interpreted the data as evidence for $T_e \sim 10^6$ K and $n_e \sim 10$ cm^{-3} gas with nearly 100% surface filling factor toward the CMZ (see Goldreich & Sridhar [2006] for a different interpretation). Rodríguez-Fernández & Martín-Pintado (2005) have observed fine structure and recombination lines toward a sample of 18 sources and reported even higher electron densities of 30–100 cm^{-3}. Lazio & Cordes (1998) inferred that these regions were at interfaces between molecular clouds and the X-ray plasma and proposed (see their Fig. 9) that the high-density molecular clouds with a volume filling factor of perhaps $f_v \sim 0.1$ are surrounded by the scattering electron gas, and the rest of the space is filled with X-ray-emitting plasma. Our observations and analysis (see also Oka et al. 2005) contradict such a picture (Boldyrev & Yusef-Zadeh 2006).

5.3. The Case of High ζ in the CMZ

It is usually assumed that the density of high-energy ($E > 100$ MeV) cosmic rays is approximately uniform over the Galaxy because of their long mean free paths. The uniform distribution on the sky of diffuse γ-ray emission appears to lend support to this (e.g., Digel et al. 2001). Recent detailed calculations by

Büsching et al. (2005) typically give a 20% variation, depending on location and time. However, the situation is very different for low-energy cosmic rays, which are the most important for ionization of the gas; their energy densities can vary greatly depending on proximity to local cosmic sources (Kulsrud & Cesarsky 1971; Spitzer & Jenkins 1975; Cesarsky 1975) because of their short mean free paths. For example, a proton of 2 MeV, which effectively ionizes hydrogen, travels only 3 pc before losing its energy in a medium with $n_H = 100$ cm^{-3} (Cravens & Dalgarno 1978). The ionization rate by low-energy cosmic rays could be proportional to the number density of the accelerating sources (supernova remnants [SNRs]; e.g., Koyama et al. 1995) and therefore have strong local variations. If the energy density of cosmic rays follows the surface density of OB stars, the cosmic-ray ionization rate would be an order of magnitude higher in the Galactic center than in the solar neighborhood (Wolfire et al. 2003). Yusef-Zadeh et al. (2002, 2007) called for an even higher local enhancement of low-energy cosmic rays in the Galactic center ($\zeta = 2 \times 10^{-14}$ s^{-1} to 5×10^{-13} s^{-1}) to account for the iron fluorescence line at 6.4 keV. Such values are much larger than those derived in the previous section using H$_3^+$. X-rays and FUV radiation from stars may also increase ζ. A factor of 10 or higher increase of ζ due to X-ray emission has even been reported in the circumstellar disk of a low-mass star (Doty et al. 2004). The enhancements could be large for the CMZ, where there are abundant intense emitters of X-rays and EUV radiation.

For the above high values of ζ, L would be quite short if equation (2) is applied. However, there are two arguments against adopting such high values of ζ. First, as argued earlier, the observed high-velocity dispersion of H$_3^+$ indicates that the gas is quite extensive rather than confined in many small clumps. This indicates that there are nonlocal sources of ionization covering an extensive region.

Second, the results of equations (1) and (2) are based on a simple linear formalism, which is a good approximation for low values of ζ. For much higher values of ζ this should be replaced by a higher-order nonlinear formalism in which $N(\mathrm{H}_3^+)$ no longer increases proportionally to ζ, but tends to saturate. This is because a high value of ζ increases not only H$_2^+$ but also electrons as discussed by Liszt (2006, 2007), electrons destroy H$_2^+$ through dissociative recombination of H$_2^+$, $\mathrm{H}_2^+ + e^- \rightarrow \mathrm{H} + \mathrm{H}$, which competes with the H$_3^+$ production reaction $\mathrm{H}_2^+ + \mathrm{H}_2 \rightarrow \mathrm{H}_3^+ + \mathrm{H}$. The former reaction, in addition to the dissociative recombination of H$_3^+$, reduces the H$_3^+$ concentration twice. It also increases $n(\mathrm{H})$ and decreases f; hence the nonlinearity. In an example given in the bottom panel of Figure 3 of Liszt (2006), a 10 times increase of ζ from 10^{-16} to 10^{-15} s^{-1} leads to only a fourfold increase of H$_3^+$ (the saturation is more severe for the top panel). The importance of saturation depends sensitively on the value of f, the fractional abundance of H$_2$. Another source of nonlinear behavior is the production of H through dissociation of H$_2$ by cosmic rays, X-rays, and EUV radiation. The rates of these processes are comparable to the rate of ionization (Glassgold & Langer 1973, 1974). Since the reproduction of H$_2$ on dust grains is slow, H accumulates in the gas and the charge exchange reaction, $\mathrm{H}_2^+ + \mathrm{H} \rightarrow \mathrm{H}_2 + \mathrm{H}^+$, which has a high rate constant of 6.4×10^{-10} cm^3 s^{-1} and will compete with the H$_3^+$-producing reaction, introducing additional nonlinearity. The increase of $n(\mathrm{H})$ and the resulting reduction of f affect the gas in several other ways, all of which make the increase of ζ ineffective in increasing H$_3^+$. While more detailed treatments of these nonlinearities have yet to be worked out, it seems unlikely to us that ζ can be larger than $\sim 3 \times 10^{-15}$ s^{-1} over extensive portions of the CMZ. Small volumes with higher ζ may well exist in the CMZ, but they would not necessarily produce a large fraction of the observed H$_3^+$.

5.4. The $+50$ km s^{-1} Absorption toward GC IRS 3

The sight line toward GC IRS 3 is special in that at $+50$ km s^{-1} local standard of rest (LSR)it has a detectable population of H$_3^+$ in the unstable (2,2) level in addition to the large populations in the (1,1) and (3,3) levels. In addition, this is the only case for which the population in the (3,3) metastable level is definitely higher than in the (1,1) ground level [see $N(3, 3)/N(1, 1)$ in Table 4]. The observable population in the (2,2) level indicates a high density and the larger population in the (3,3) level than in the (1,1) level indicates a high-temperature environment. Our analysis yields $n = 175$–300 cm^{-3} and $T = 350$–500 K. As seen from Figure 4, this environment is clearly distinct from those elsewhere. We speculate below on two possible locations for this gas: (1) the circumnuclear disk (CND), and (2) the "50 km s^{-1} cloud" behind the Galactic center.

5.4.1. Circumnuclear Disk

GC IRS 3 is only 5″ (0.2 pc) from Sgr A*, which is well within the projected span of the Central cluster (the maximum transverse separation of bright stars in the cluster is $\sim$0.65 pc; Viehmann et al. 2005). The central 3 pc of the Galactic center contains hot, high-density gas which shows intricate minispiral structures (Ekers et al. 1983; Lo & Claussen 1983) termed the Western Arc, the Northern Arm, the Eastern Arm, and the Bar (Güsten et al. 1987). The extension of the Western Arc has been associated with a nearly completely circular, Keplerian circumnuclear disk by analysis of HCN radio emission (Güsten et al. 1987; Genzel & Townes 1987; Jackson et al. 1993; Christopher et al. 2005) and by other methods; recent direct observations of the disk via its far-infrared dust emission by Latvakoski et al. (1999) are particularly noteworthy. There also have been attempts to interpret other three minispirals as CNDs that are not necessarily elliptical (e.g., Liszt et al. 1985; Quinn & Sussman 1985; Lacy et al. 1991; Jackson et al. 1993; Liszt 2003). GC IRS 3 is located in the cavity between the Northern Arm and the Bar, a region of low gas density. H. S. Liszt (2008, private communication) has suggested that the H I absorption at $+50$ km s^{-1} in Figure 5 of Liszt et al. (1985) may be due to the same cloud producing the H$_3^+$ absorption in the sight line toward GC IRS 3. Not only does the velocity match, but also the high-velocity gradient of 100 km s^{-1} arcmin^{-1} found by Liszt et al. (1985) is consistent with the width of the H$_3^+$ 50 km s^{-1} absorption feature.

However, there are two possible problems with this interpretation. First, it calls for an uncomfortably high cosmic ionization rate in order to account for the observed H$_3^+$ column density in the short path length within the CND. Assuming a path length on the order of 0.5 pc, the observed $(\zeta L)_{\min}$ of 7.5×10^4 cm s^{-1} in Table 4 gives $\zeta \sim 2 \times 10^{-14}$ s^{-1}, an extremely high value. Such a value is possible (Yusef-Zadeh et al. 2007) in view of the high density of stars and radiation field in the region, but in such conditions the higher order chemistry (Liszt 2006, 2007) discussed in § 5.3 surely plays a role. Although the detection of H$_3^+$ in the unstable (2,2) level indicates higher density compared with other sight lines, the population of the (3,3) level is still much higher, and the distribution is highly nonthermal. The density is definitely much lower than that reported for the CND (10^4–10^6 cm^{-3}). This could be due to the fact that GC IRS 3 is in the northern cavity and is only behind the edge of the CND rather than behind its densest regions.

The second problem is the absence of the $R(2, 2)^l$ line in the spectrum of GC IRS 1W. It is remarkable that the $R(2, 2)^l$ line is detected toward GC IRS 3 but not toward GC IRS 1W, which is just 8.4″ away, or 0.31 pc for a common distance of 7.6 kpc (Eisenhauer et al. 2005; Nishiyama et al. 2006). If both stars

belong to the Central cluster (Becklin et al. 1978; Viehmann et al. 2005), it is not likely that they are much more than 0.5 pc apart. Although the source might well be located in the foreground, GC IRS 1W overlaps with the high-density part of the Northern Arm, while GC IRS 3 is located in the cavity. It is difficult to understand why only GC IRS 3 shows $R(2, 2)^l$ absorption, if the absorption occurs within the CND.

5.4.2. *The "50 km s^{-1} Cloud"*

The observed velocity of +50 km s^{-1} toward GC IRS3 immediately suggests that the absorption might arise in the well-known "50 km s^{-1} cloud," one of the giant molecular clouds ($>10^6\ M_\odot$) located near the Galactic center. The "50 km s^{-1} cloud" is sometimes referred to as M$-0.02-0.07$, was called the "40 km s^{-1} cloud" by Oort (1977), and has been discussed in detail by Brown & Liszt (1984). Many atomic and molecular studies have established that it is located *behind* the Galactic nucleus, in between the nonthermal radio source Sgr A East (SNR) and the H II region Sgr A West, which enshrouds the central star cluster (Whiteoak et al. 1974; Güsten & Henkel 1983; Pauls et al. 1996). Yusef-Zadeh et al. (1996) argued that the several masers they discovered in the southeast of Sgr A* are excited in the shock-heated interface between Sgr A East and M$-0.02-0.07$, where the expanding supernova remnant hits the giant molecular cloud. Tsuboi et al. (2006) also found clues for an interaction between Sgr A East and the "50 km s^{-1} cloud" in the high-velocity wings of CS $J = 1-0$, although it may not be the case that the "50 km s^{-1} cloud" is the sole cloud that falls in the radial velocity +50 km s^{-1} in the line of sight toward the Galactic center (Zylka et al. 1992).

Geballe et al. (1989) found that GC IRS 3 and IRS 7 show deep absorption lines of the CO fundamental band at 4.7 μm at the radial velocity +50 km s^{-1}, while GC IRS 1 and IRS 2 do not. They attributed the +50 km s^{-1} absorption to the CND but also mentioned the possibility that GC IRS 3 is not a member of the central cluster, but behind the +50 km s^{-1} cloud and thus not in the Central cluster. The nature of GC IRS 3 is controversial (Pott et al. 2008); it is among the brightest sources in the Central cluster region, only less luminous than GC IRS 1 and GC IRS 10, and much redder than them in the mid-infrared even though it is (apparently) in the cavity. Because of its location and featureless infrared continuum (e.g., Krabbe et al. 1995), GC IRS 3 has widely been believed to be a hot massive star heavily obscured by its own dust (similar to the bright Quintuplet sources), in addition to foreground dust. However, new interferometric observations that resolve the circumstellar dust shell have been interpreted by Pott et al. (2008) as evidence that the central object is a late-type carbon star, the photospheric spectral features of which are completely obscured. This interpretation is consistent with the apparent lack of ionization of the circumstellar shell, which one might expect if the object lies within the Central cluster, and indeed with the lack of ionized gas near GC IRS 3 (Roche & Aitken 1985). Although somewhat unlikely due to its proximity on the plane of the sky to the Central cluster, the placement of GC IRS 3 well behind the cluster and the "+50 km s^{-1} cloud" is otherwise a straightforward assignment and avoids the difficulties associated with the CND hypothesis mentioned in the previous section.

5.5. *Infrared Pumping*

During the 2005 Royal Society Discussion Meeting on H$_3^+$ (Oka 2006a), J. H. Black proposed an infrared pumping mechanism that can produce a nonthermal rotational level distribution of H$_3^+$ if the infrared flux is sufficiently high. The mechanism is illustrated in Figure 5. Infrared radiation pumps H$_3^+$ from the fully populated lowest ortholevel, (1,0), to the (2,0) level in the first excited vi-
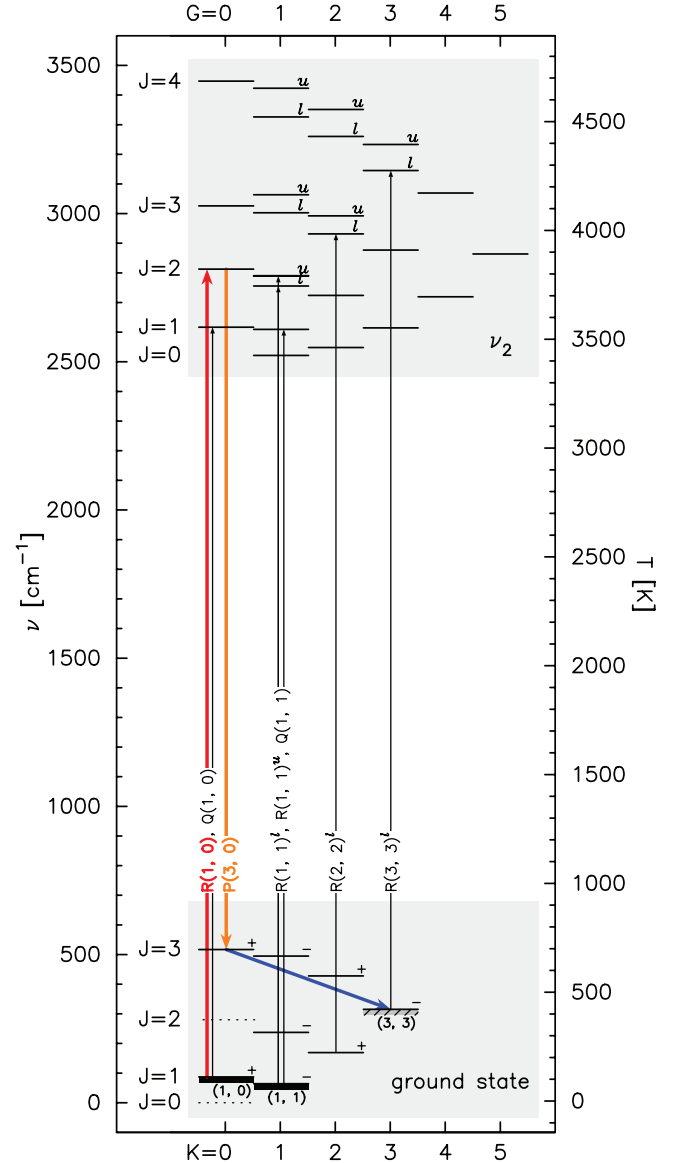

FIG. 5.— Schematic of the infrared pumping mechanism proposed by J. H. Black. H$_3^+$ in the lowest ortholevel (1,0) is excited to the (2,0) level in the first excited vibrational state via the $R(1, 0)$ transition (*red line*) by ambient photons. The excited H$_3^+$ spontaneously decays to the (3,0) ground level through the $P(3, 0)$ transition (*orange line*) and then to the metastable (3,3) level (*blue line*). See text for more details. Other transitions used in this paper are also shown.

brational state via the $R(1,0)$ transition. The molecule decays to the (3,0) level in the ground state by spontaneous emission with a lifetime of 25.3 ms. The molecule further decays to the (3,3) metastable level through the forbidden rotational transition $(3, 0) \rightarrow (3, 3)$ emitting a far-infrared photon at 49.62 μm in 3.75 hr (Pan & Oka 1986; Neale et al. 1996). Thus, H$_3^+$ molecules are pumped from the (1,0) level to the metastable (3,3) level.

Since the spontaneous emissions are all very fast, the rate-determining process for Black's mechanism is the rate of infrared pumping of the (1,0) level of H$_3^+$. We rewrite the excitation rate given in equation (15) of van Dishoeck & Black (1982) as

$$W_{R(1,0)} = \lambda^2 A \phi_\nu / 8\pi = 1.51 \times 10^{-7} \phi_\nu \ \mathrm{s}^{-1},$$

where ϕ_ν is the photon flux of the ambient radiation at the wavelength of the transition in the units of photon cm^{-2} s^{-1} Hz^{-1}, and

the value of $\lambda = 3.6685$ μm, the Einstein coefficient $A = 98.5$ s^{-1}, and the dilution factor of 0.286 are used. The dilution factor takes into account the spontaneous emission $(2, 0) \rightarrow (1, 0)$ back to the ground level $(1,1)$ with $A = 35.5$ s^{-1}, resulting in a reduction of the pumping efficiency. In order for pumping to be significant, the value of $W_{R(1,0)}$ has to be comparable to the collision rate,

$$R = n\sigma v = nk_L \sim 2 \times 10^{-7} \text{ s}^{-1},$$

where we used a number density of $n = 100$ cm^{-3} and the temperature-independent Langevin rate constant, 2×10^{-9} cm^3 s^{-1} for the $H_3^+ + H_2$ collision.

The energy density of the interstellar radiation field in the solar neighborhood at 4 μm has been estimated by Porter et al. (2006) to be $\lambda u_\lambda = 0.055$ μm eV cm^{-3} μm^{-1}, which translates to $\phi_\nu = 6 \times 10^{-5}$ photons cm^{-2} s^{-1} Hz^{-1}. This is consistent with the value reported by Mathis et al. (1983) within a factor of 1.5. The corresponding pumping rate is $W_{R(1,0)} = 1 \times 10^{-11}$ s^{-1}, about 2×10^4 times lower than the collision rate. Porter et al. (2006) have estimated an average energy density about 20 times higher in the Galactic center. Launhardt et al. (2002) have reported an energy density in the central 120 pc (their Fig. 10) which is another factor of 10 higher. The corresponding pumping rate is still 100 times lower than the collision rate and the infrared pumping is perhaps not very effective for the majority of the gas reported in this paper.

In the central parsec of the Galaxy, however, the stellar density is $\sim 10^6$ $M_\odot$ pc^{-3} (Schödel et al. 2007), including a large number of luminous red giants and at least 80 hot and massive stars (Paumard et al. 2006). In this environment infrared pumping likely would overwhelm the collisional relaxation of any H_3^+ that is present. The effect, however, must be local to the very central region of the CMZ and probably does not seriously alter the population of the (3,3) level beyond a few tens of parsecs from the center, i.e., in the bulk of the CMZ. However, it may well be the best explanation for the strong $R(3,3)^l$ absorption line toward GC IRS 3 at 50 km s^{-1} discussed in the previous subsection.

6. SUMMARY POINTS

1. Seven infrared spectral lines of H_3^+, $Q(1,0)$, $Q(1,1)$, $R(1,1)^l$, $R(1,0)$, $R(1,1)^u$, $R(2,2)^l$, and $R(3,3)^l$, have been observed toward eight bright and hot stars distributed from the Quintuplet cluster ~ 30 pc east of the Galactic center to the Central cluster close to Sgr A*, using the IRCS spectrograph of the Subaru Telescope.

2. All sight lines showed strong $R(3,3)^l$ absorptions with high-velocity dispersions, indicating a high population of the (3,3) metastable rotational level. Those absorptions are ascribed to H_3^+ in the CMZ and indicate a large surface filling factor.

3. The five absorption lines starting from the lowest levels, $(1,1)$ and $(1,0)$, are composed of sharp spectral lines due to H_3^+ in the foreground spiral arms and a broad trough due to H_3^+ in the CMZ. These two absorption components have been separated by assuming that the profile of the trough is proportional to the $R(3,3)^l$ absorption profile.

4. The observed high H_3^+ column densities indicate lower limits of ζL, $(\zeta L)_{min} = (1.3–4.5) \times 10^5$ cm s^{-1}, which are 1000 and

10 times higher than for dense and diffuse clouds in the Galactic disk, respectively, indicating high values of ζ and L in the CMZ.

5. Various arguments suggest ζ is on the order of 10^{-15} s^{-1} and L on the order of 50 pc in the CMZ, indicating a high ionization rate in the region and a high volume filling factor of the gas.

6. Analysis based on the thermalization model calculation (Oka & Epp 2004) has given $T = 200–300$ K and $n \leq 50–200$ cm^{-3} (Fig. 4). A lower limit on the order of 50 cm^{-3} is set for n from the observed visual extinction, A_V, and the existence of detectable H_3^+.

7. Taken as a whole, the observations reveal a previously unidentified gaseous environment in the CMZ having a high volume filling factor. This is radically different than the previous picture of the gas in the CMZ, and suggests in particular that the filling factor of ultrahot X-ray emitting plasma may be nowhere close to unity.

8. The sight line toward GC IRS 3, close to Sgr A*, is unique in having a detectable population in the H_3^+ (2,2) unstable level near +50 km s^{-1}, indicating a higher density for the gas producing this absorption. We speculate that the cloud responsible for this absorption feature is either a compact cloud near the circumnuclear disk or the well-known "50 km s^{-1} cloud." For the former a high value of $\zeta = 2 \times 10^{-14}$ s^{-1} is needed, while for the latter GC IRS 3 is located behind the "50 km s^{-1} cloud" and thus outside of the Central cluster.

9. An infrared pumping mechanism, proposed by J. H. Black to populate the (3,3) metastable level, has been examined. The infrared radiation in the extended CMZ is not intense enough to significantly pump this level, and the high temperatures detected there are likely thermal. However, in the CND pumping probably dominates and temperatures determined for gas in that region based on the relative populations in this level and the $J = 1$ levels would not be kinetic temperatures.

REFERENCES

Amano, T. 1988, ApJ, 329, L121
Arimoto, N., Sofue, Y., & Tsujimoto, T. 1996, PASJ, 48, 275
Becklin, E. E., Matthews, K., Neugebauer, G., & Willner, S. P. 1978, ApJ, 219, 121
Black, J. H., & Dalgarno, A. 1977, ApJS, 34, 405
Bohlin, R. C., Savage, B. D., & Drake, J. F. 1978, ApJ, 224, 132
Boldyrev, S., & Yusef-Zadeh, F. 2006, ApJ, 637, L101

Bolton, J. G., Gardner, F. F., McGee, R. X., & Robinson, B. J. 1964, Nature, 204, 30
Brown, R. L., & Liszt, H. S. 1984, ARA&A, 22, 223
Büsching, I., Kopp, A., Pohl, M., Schlickeiser, R., Perrot, C., & Grenier, I. 2005, ApJ, 619, 314
Cesarsky, C. J. 1975, in Proc. 14th Int. Cosmic Ray Conf. (München: MPI), 634

Christopher, M. H., Scoville, N. Z., Stolovy, S. R., & Yun, M. S. 2005, ApJ, 622, 346
Cotera, A. S., Simpson, J. P., Erickson, E. F., & Colgan, S. W. J. 1999, ApJ, 510, 747
Cotera, A. S., Simpson, J. P., Erickson, E. F., Colgan, S. W. J., Burton, M. G., & Allen, D. A. 2000, ApJS, 129, 123
Cravens, T. E., & Dalgarno, A. 1978, ApJ, 219, 750
Dahmen, G., Hüttemeister, S., Wilson, T. L., & Mauersberger, R. 1998, A&A, 331, 959
Dalgarno, A. 2006, Proc. Natl. Acad. Sci., 103, 12269
Digel, S. W., Grenier, I. A., Hunter, S. D., Dame, T. M., & Thaddeus, P. 2001, ApJ, 555, 12
Doty, S. D., Schöier, F. L., & van Dishoeck, E. F. 2004, A&A, 418, 1021
Eisenhauer, F., et al. 2005, ApJ, 628, 246
Ekers, R. D., van Gorkom, J. H., Schwarz, U. J., & Goss, W. M. 1983, A&A, 122, 143
Field, G. B., Goldsmith, D. W., & Habing, H. J. 1969, ApJ, 155, L149
Figer, D. F. 2004, in ASP Conf. Ser. 322, The Formation and Evolution of Massive Young Star Clusters, ed. H. J. G. L. M. Lamers, L. J. Smith, & A. Nota (San Francisco: ASP), 49
Figer, D. F., McLean, I. S., & Morris, M. 1999, ApJ, 514, 202
Geballe, T. R., Baas, F., & Wade, R. 1989, A&A, 208, 255
Geballe, T. R., McCall, B. J., Hinkle, K. H., & Oka, T. 1999, ApJ, 510, 251
Geballe, T. R., & Oka, T. 1996, Nature, 384, 334
Genzel, R., Hollenbach, D., & Townes, C. H. 1994, Rep. Prog. Phys., 57, 417
Genzel, R., & Townes, C. H. 1987, ARA&A, 25, 377
Glassgold, A. E., & Langer, W. D. 1973, ApJ, 186, 859
———. 1974, ApJ, 193, 73
Goldreich, P., & Sridhar, S. 2006, ApJ, 640, L159
Goto, M., McCall, B. J., Geballe, T. R., Usuda, T., Kobayashi, N., Terada, H., & Oka, T. 2002, PASJ, 54, 951
Güsten, R., Genzel, R., Wright, M. C. H., Jaffe, D. T., Stutzki, J., & Harris, A. I. 1987, ApJ, 318, 124
Güsten, R., & Henkel, C. 1983, A&A, 125, 136
Hartquist, T. W., Doyle, H. T., & Dalgarno, A. 1978, A&A, 68, 65
Hayakawa, S., Nishimura, S., & Takayanagi, K. 1961, PASJ, 13, 184
Indriolo, N., Geballe, T. R., Oka, T., & McCall, B. J. 2007, ApJ, 671, 1736
Jackson, J. M., Geis, N., Genzel, R., Harris, A. I., Madden, S., Poglitsch, A., Stacey, G. J., & Townes, C. H. 1993, ApJ, 402, 173
Kobayashi, N., et al. 2000, Proc. SPIE, 4008, 1056
Koyama, K., Awaki, H., Kunieda, H., Takano, S., Tawara, Y., Yamauchi, S., Hatsukade, I., & Nagase, F. 1989, Nature, 339, 603
Koyama, K., Maeda, Y., Sonobe, T., Takeshima, T., Tanaka, Y., & Yamauchi, S. 1996, PASJ, 48, 249
Koyama, K., Petre, R., Gotthelf, E. V., Hwang, U., Matsuura, M., Ozaki, M., & Holt, S. S. 1995, Nature, 378, 255
Koyama, K., et al. 2007, PASJ, 59, S245
Krabbe, A., et al. 1995, ApJ, 447, L95
Kulsrud, R. M., & Cesarsky, C. J. 1971, Astrophys. Lett., 8, 189
Lacy, J. H., Achtermann, J. M., & Serabyn, E. 1991, ApJ, 380, L71
Lacy, J. H., Knacke, R., Geballe, R., & Tokunaga, A. T. 1994, ApJ, 428, L69
Larsson, M. 2000, Philos. Trans. R. Soc. London A, 358, 2433
Larsson, M., et al. 1993, Phys. Rev. Lett., 70, 430
Latvakoski, H. M., Stacey, G. J., Gull, G. E., & Hayward, T. L. 1999, ApJ, 511, 761
Launhardt, R., Zylka, R., & Mezger, P. G. 2002, A&A, 384, 112
Lazio, T. J. W., & Cordes, J. M. 1998, ApJ, 505, 715
Linke, R. A., Stark, A. A., & Frerking, M. A. 1981, ApJ, 243, 147
Liszt, H. S. 2003, A&A, 408, 1009
———. 2006, Philos. Trans. R. Soc. London A, 364, 3049
———. 2007, A&A, 461, 205
Liszt, H. S., Burton, W. B., & van der Hulst, J. M. 1985, A&A, 142, 237
Lo, K. Y., & Claussen, M. J. 1983, Nature, 306, 647
Lord, S. D. 1992, A New Software Tool for Computing Earth's Atmosphere Transmissions of Near- and Far-Infrared Radiation, NASA Technical Memoir 103957 (Moffett Field: NASA Ames Research Center)
Markevitch, M., Sunyaev, R. A., & Pavlinsky, M. 1993, Nature, 364, 40
Mathis, J. S., Mezger, P. G., & Panagia, N. 1983, A&A, 128, 212
McCall, B. J., Geballe, T. R., Hinkle, K. H., & Oka, T. 1998, Science, 279, 1910
———. 1999, ApJ, 522, 338
McCall, B. J., et al. 2002, ApJ, 567, 391
———. 2003, Nature, 422, 500
———. 2004, Phys. Rev. A, 70, 052716

Mezger, P. G., Duschl, W. J., & Zylka, R. 1996, A&A Rev., 7, 289
Moneti, A., Glass, I., & Moorwood, A. 1992, MNRAS, 258, 705
Morris, M. 2006, J. Phys. Conf. Ser., 54, 1
Morris, M., & Nayakshin, S. 2006, J. Phys. Conf. Ser., 54, 461
Morris, M., & Serabyn, E. 1996, ARA&A, 34, 645
Muno, M. P., Bower, G. C., Burgasser, A. J., Baganoff, F. K., Morris, M. R., & Brandt, W. N. 2006, ApJ, 638, 183
Muno, M. P., et al. 2003, ApJ, 589, 225
———. 2004, ApJ, 613, 326
Nagata, T., Hyland, A. R., Straw, S. M., Sato, S., & Kawara, K. 1993, ApJ, 406, 501
Nagata, T., Woodward, C. E., Shure, M., & Kobayashi, N. 1995, AJ, 109, 1676
Nagata, T., Woodward, C. E., Shure, M., Pipher, J. L., & Okuda, H. 1990, ApJ, 351, 83
Neale, L., Miller, S., & Tennyson, J. 1996, ApJ, 464, 516
Nishiyama, S., et al. 2006, ApJ, 647, 1093
O'Donnell, E. J., & Watson, W. D. 1974, ApJ, 191, 89
Oka, T. 2006a, Philos. Trans. R. Soc. London A, 364, 2847
———. 2006b, Proc. Natl. Acad. Sci., 103, 12235
Oka, T., & Epp, E. 2004, ApJ, 613, 349
Oka, T., Geballe, T. R., Goto, M., Usuda, T., & McCall, B. J. 2005, ApJ, 632, 882
Oka, T., Hasegawa, T., Hayashi, M., Handa, T., & Sakamoto, S. 1998a, ApJ, 493, 730
Oka, T., Hasegawa, T., Sato, F., Tsuboi, M., & Miyazaki, A. 1998b, ApJS, 118, 455
Okuda, H., et al. 1990, ApJ, 351, 89
Oort, J. H. 1977, ARA&A, 15, 295
Ott, T., Eckart, A., & Genzel, R. 1999, ApJ, 523, 248
Padoan, P., & Scalo, J. 2005, ApJ, 624, L97
Palmer, P., Zuckerman, B., Buhl, D., & Snyder, L. E. 1969, ApJ, 156, L147
Pan, F.-S., & Oka, T. 1986, ApJ, 305, 518
Pauls, T., Johnston, K. J., & Wilson, T. L. 1996, ApJ, 461, 223
Paumard, T., et al. 2006, ApJ, 643, 1011
Porter, T. A., Moskalenko, I. V., & Strong, A. W. 2006, ApJ, 648, L29
Pott, J.-U., Eckart, A., Glindemann, A., Schödel, R., Viehmann, T., & Robberto, M. 2008, A&A, 480, 115
Quinn, P. J., & Sussman, G. J. 1985, ApJ, 288, 377
Revnivtsev, M., Sazonov, S., Gilfanov, M., Churazov, E., & Sunyaev, R. 2006, A&A, 452, 169
Roche, P. F., & Aitken, D. K. 1985, MNRAS, 215, 425
Rodríguez-Fernández, N. J., & Martín-Pintado, J. 2005, A&A, 429, 923
Sawada, T., Hasegawa, T., Handa, T., & Cohen, R. J. 2004, MNRAS, 349, 1167
Schödel, R., et al. 2007, A&A, 469, 125
Sodroski, T. J., et al. 1995, ApJ, 452, 262
Sofia, U. J., Lauresch, J. T., Myers, D. M., & Cartledge, S. I. B. 2004, ApJ, 605, 272
Spitzer, L., Jr., & Jenkins, E. B. 1975, ARA&A, 13, 133
Spitzer, L., Jr., & Tomasko, M. G. 1968, ApJ, 152, 971
Sunyaev, R. A., Markevitch, M., & Pavlinsky, M. 1993, ApJ, 407, 606
Takami, H., et al. 2004, PASJ, 56, 225
Tanner, A., et al. 2006, ApJ, 641, 891
Tokunaga, A. T., et al. 1998, Proc. SPIE, 3354, 512
Tsuboi, M., Okumura, S. K., & Miyazaki, A. 2006, J. Phys. Conf. Ser., 54, 16
van Dishoeck, E. F., & Black, J. H. 1982, ApJ, 258, 533
———. 1986, ApJS, 62, 109
Viehmann, T., Eckart, A., Schödel, R., Moultaka, J., Straubmeier, C., & Pott, J.-U. 2005, A&A, 433, 117
Wang, Q. D., Gotthelf, E. V., & Lang, C. C. 2002, Nature, 415, 148
Warwick, R., Sakano, M., & Decourchelle, A. 2006, J. Phys. Conf. Ser., 54, 103
Webber, W. R. 1998, ApJ, 506, 329
Whiteoak, J. B., Rogstad, D. H., & Lockhart, I. A. 1974, A&A, 36, 245
Whittet, D. C. B., et al. 1997, ApJ, 490, 729
Wolfire, M. G., McKee, C. F., Hollenbach, D., & Tielens, A. G. G. M. 2003, ApJ, 587, 278
Yamauchi, S., & Koyama, K. 1993, ApJ, 404, 620
Yusef-Zadeh, F., Law, C., & Wardle, M. 2002, ApJ, 568, L121
Yusef-Zadeh, F., Muno, M., Wardle, M., & Lis, D. C. 2007, ApJ, 656, 847
Yusef-Zadeh, F., Roberts, D. A., Goss, W. M., Frail, D. A., & Green, A. J. 1996, ApJ, 466, L25
Zylka, R., Mezger, P. G., & Lesch, H. 1992, A&A, 261, 119